CONF-920768--8

Experimental demonstration of high resolution three-dimensional x-ray holography

I. McNulty
Advanced Photon Source, Argonne National Laboratory, Argonne, IL 60439

J.E. Trebes, J.M. Brase, T.J. Yorkey, R. Levesque, and H. Szoke
Lawrence Livermore National Laboratory, Livermore, CA 94550

E.H. Anderson
Lawrence Berkeley Laboratory, Berkeley, CA 94720

C. Jacobsen
Physics Department, State University of New York, Stony Brook, NY 11794

D. Kern
IBM T.J. Watson Research Laboratory, Yorktown Heights, NY 10598

ANL/XFD/CP--76139

DE93 004178

ABSTRACT

Tomographic x-ray holography may make possible the imaging of biological objects at high resolution in three dimensions. We performed a demonstration experiment with soft x-rays to explore the feasibility of this technique. Coherent 3.2-nm undulator radiation was used to record Fourier transform holograms of a microfabricated test object from various illumination angles. The holograms were numerically reconstructed according to the principles of diffraction tomography, yielding images of the object that are well resolved in three dimensions.

1. INTRODUCTION

X-ray holographic microscopy is rapidly developing as a promising tool for high resolution study of biological objects. It is potentially capable of three-dimensional resolution, it is amenable to flash sources, and it might be used to investigate, for example, the internal organization of subcellular organelles and the higher-order structure of macromolecules such as DNA. In particular, the use of soft x-rays as a probe offers finer spatial resolution to optical techniques and lower radiation dose than electron microscopy. X-ray wavelengths of 2.3-4.5 nm are well suited to the study of thick, wet, unstained, initially living specimens.[1-3]

Soft x-ray holography has recently been demonstrated by Howells,[4] Jacobsen,[5] Joyeux,[6] and McNulty[7] using undulator radiation, and by Trebes[8] using an x-ray laser. Two hologram recording schemes have been utilized: the Gabor in-line geometry[9] and the Fourier transform geometry.[10,11] Using both arrangements, the best x-ray holograms obtained to date have good (<100 nm) transverse resolution; however, they display little or no longitudinal resolution due to their limited numerical aperture.

Clearly, the development of flash x-ray holography with a three-dimensional (3D) resolution of 10-30 nm would have major implications for structural biology. In holography as well as in other types of imaging, the transverse and longitudinal resolution δ_t and δ_ℓ depend on the wavelength λ and the numerical aperture NA by

$$\delta_t = \alpha_t \frac{\lambda}{NA} \tag{1}$$

$$\delta_\ell = \alpha_\ell \frac{\lambda}{(NA)^2} \tag{2}$$

DISCLAIMER

where α_t and α_ℓ are constants of order 1 specific to the shape of the aperture and to the resolution criteria applied. The largest angle over which fringes in the hologram are recorded with high visibility determines the NA. But, obtaining large NA with x-rays is difficult due to the near-unity refractive index of matter. In biological specimens, x-ray photons are absorbed, pass straight through, or are mostly scattered through relatively small angles.

Diffraction tomography (DT) is an alternative approach to 3D imaging in which several holograms of the specimen are recorded from various illumination directions and combined in the reconstruction step.[12,13] This permits the specimen to be sampled over a wide range of spatial frequencies to improve the depth resolution in cases where, as for x-rays, the scattered radiation is predominantly forward-directed. Diffraction tomography is an extension of ordinary (e.g. medical) tomographic methods, although in principle, fewer projections are required to form 3D images by DT because each hologram contains considerable transverse and some depth information. The depth resolution attainable by tomographic means depends on the complexity of the object as well as the number and aperture of the assembled projections. The optimum number of holographic projections is necessarily a compromise between maximizing the depth resolution and signal-to-noise ratio while minimizing the radiation dose to the specimen.

This paper discusses an experimental demonstration of soft x-ray DT and the initial results. The ultimate objectives of this work are to assess the number of holographic views necessary to achieve comparable depth and transverse resolution with 3D specimens, and to determine the number of x-rays required to record the holograms with adequate signal-to-noise ratios for accurate tomographic reconstruction.

2. EXPERIMENT

The experiment was conducted as follows. Fourier transform holograms of an artificial test object were recorded with a CCD camera from various directions by orienting the object with respect to the camera and the incident x-ray beam on a rotatable stage. The holograms were then reconstructed a[illegible]ssembled by computer according to the principles of DT to obtain 3D images of the object. The optical setup (see Fig. 1) is similar to the arrangement used previously in two-dimensional holography experiments,[7,14] however, due to the additional degree of freedom needed, we sought to simplify alignment of the optics and to record more easily interpretable holograms. Consequently, we used an uncomplicated test object consisting of two closely spaced parallel bars to generate both the object and the reference waves. Coherent x-rays scattered by the two bars interfere to produce a Young's fringe pattern that may be thought of as the Fourier transform hologram of one of the bars.

The X1 soft x-ray undulator and X1A beamline at the National Synchrotron Light Source provided the coherent x-ray beam.[15] The spectral brightness of the undulator is approximately 10^{17} photons/s/mm^2/mrad^2 per 0.1% bandwidth; the beamline efficiency is about 6% for 2-5 nm x-rays. In this wavelength range, the beamline typically delivers a spatially coherent flux of 5×10^8 photons/s to the experiment in a spectral bandwidth of 0.2-0.5%.

For test objects, we deposited metal patterns onto silicon nitride membranes by electron beam lithography.[16] The object used in this work (Fig. 2) is made of gold. The bars are 90 nm thick, 130 nm wide, 230 μm long, and are spaced 2.5 μm apart. The soft x-ray transmission of the 100-nm-thick supporting membrane is best (70%) at a wavelength of 3.2 nm. The opacity of the bars at this wavelength is 91%. The test object was mounted on a small stage with three linear axes and one rotational axis; the positioning precision of the stage was ±2 μm and ±0.1°. It was inserted into the x-ray beam in a ~5 mm gap between the beamline exit window and the detector entrance window. The gap was flushed with helium to diminish absorption of the x-ray beam in air. A gas flow proportional counter was used to check the alignment of the specimen in the beam and to measure the incident and transmitted x-ray flux.

A low-noise CCD camera recorded the holograms in digital form.[14] Its noise-equivalent exposure is about fifteen soft x-ray photons. Because the camera is cooled with liquid nitrogen, the dark current is negligible for exposures up to an hour in duration. The CCD array is a single field of 576 by 384 pixels, 23 μm by 23 μm in size. Inside the camera, suspended by fine wires in front of the CCD, is a 2-mm-square photoconductive diamond (PCD) detector. The PCD serves as a stop to block the intense zero-order beam which is transmitted unscattered by the specimen, preventing saturation of the CCD. It is also used to monitor the incoming beam during hologram exposures. The soft x-ray performance of the CCD camera was calibrated against the proportional counter by measuring the direct beam through a 1-μm-thick tin filter.

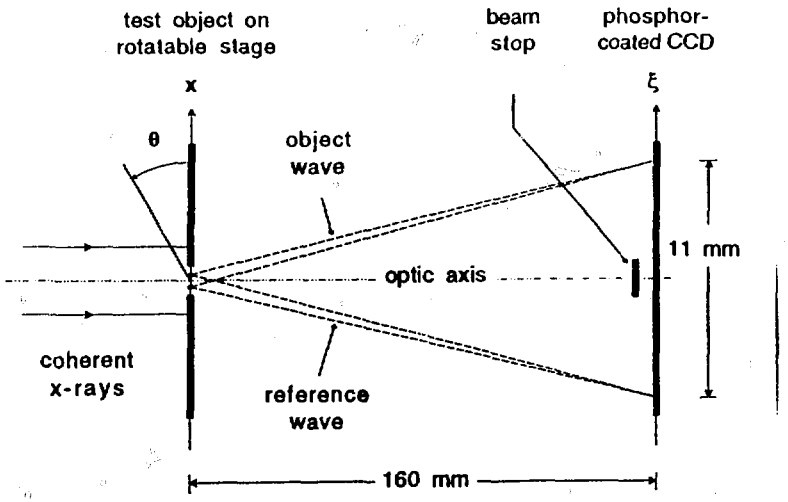

Fig. 1. Schematic diagram of the experiment. A coherent x-ray beam illuminates the double-bar test object (shown end-on). X-rays scattered from the bars form the hologram: one bar generates the reference wave and the other bar generates the object wave. A CCD camera records the interference of the two waves. X-rays which are not absorbed or scattered by the specimen are blocked by the beam stop to prevent saturation of the CCD.

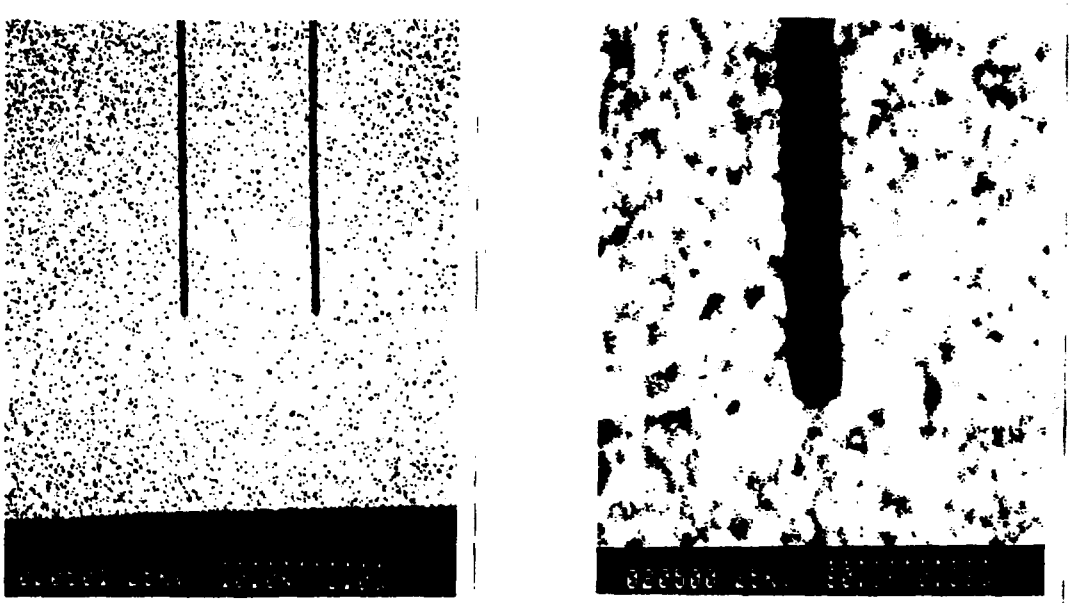

(a) (b)

Fig. 2. Scanning electron micrographs of the test object: (a) view at low magnification, (b) close-up of one bar.

McNully

3. X-RAY HOLOGRAMS

Two soft x-ray holograms of the test object recorded with the object oriented at different angles with respect to the incident beam are shown in Fig. 3. The beamline monochromator was set to a wavelength of 3.2 nm. An exposure time of one minute was sufficient to record high contrast fringes. In the holograms, one can see a distinct fringe structure, a more diffuse signal near the center, and the shadow of the PCD (dark square region). The diffuse low-angle component is due to scattering of the x-ray beam by the various apertures in the system. The left-to-right width of the interference fringes corresponds to the length of the bars. The bar width determines the extent of the overall envelope, and the bar spacing determines the fringe period. In the Fresnel approximation,[17] the amplitude at the detector along the axis normal to the bars, with the bars oriented perpendicular to the beam, is given by

$$a(\xi) = \frac{e^{ikz}}{i\lambda z}\left\{\int_{-a}^{a} e^{\frac{ik}{2z}(x-\xi)^2}\,dx - \int_{-d-b}^{-d+b} e^{\frac{ik}{2z}(x-\xi)^2}\,dx - \int_{d-b}^{d+b} e^{\frac{ik}{2z}(x-\xi)^2}\,dx\right\}, \qquad (3)$$

where 2a is the width of the aperture enclosing the bars, 2b is the bar width, 2d is the bar spacing, x and ξ are spatial coordinates in the object and hologram planes, z is the distance between the two planes, and $k = 2\pi/\lambda$. The first term corresponds to the field diffracted by the aperture and the latter two terms correspond to the diffracted fields due to the bars. The integration limits and dependence on z are modified when the object is rotated with respect to the beam and detector.

Fig. 4 compares a line scan taken through the center of the hologram in Fig. 3(a) with the irradiance $|a(\xi)|^2$ calculated via Eq. 3 for this test object. The fringe spacing of 205 μm and envelope width of ~4 mm are consistent with the calculated pattern. Due to insufficient angular acceptance of the camera entrance window, the weaker second-order peaks visible in Fig. 4(b) were cut off and not recorded. The central peak was blocked by the PCD. The fringe visibility in the x-ray hologram is nearly 100%. Although modest, the spatial coherence width (50 μm) and longitudinal coherence length (0.6 μm) of the incident x-ray beam was more than adequate for good visibility due to the small path differences involved.

With a current of 150 mA in the storage ring, the flux incident on the test object was 4×10^3 photons/μm²/s as measured using the proportional counter. A total of 2×10^{10} photons was required to record each minute-long hologram. Most of the incident x-rays were not scattered by the object and reference bars and thus did not contribute to the information-carrying terms in the holograms; this component was intercepted by the PCD.

4. RECONSTRUCTIONS IN 3D

Fig. 5 shows numerical reconstructions of 1-μm segments of the test object from four oblique views. The images were obtained from three holographic views recorded with the test object at normal incidence (0°), +45°, and −45° to the beam. The holograms were first reconstructed by 3D phase recovery and Fourier transformation, then the individual reconstructions were assembled to produce the 3D images shown.[18,19] Although the intrinsic field of view of the holograms is about 10 μm in diameter, the reconstructed portion of the bar was limited to a length of 1 μm to save computer time (it also supplies a convenient scale). The pixel size is 15.6 nm. The most prominent feature of the reconstructions is that the object is uniformly well resolved over its extent and is well localized in 3-space, evidence that the reconstruction algorithm effectively suppresses artifacts. Because one of the bars provided the reference wave, only the "object" bar is evident in the reconstructions.

To reconstruct the object wave accurately in 3D, the object and reference locations should be known for each hologram to a fraction of a wavelength. Not only is this impractical, registration of the holograms is made difficult by the fact that it is impossible to rotate through large angles without introducing small errors in the object position. Furthermore, the location of the reference source with respect to the object source depends on the angular orientation on the bars. To reduce the registration problem, we carefully prealigned the test object for each hologram exposure using visible-light optics. The registry of the reconstructed holograms was fine-tuned in software by aligning the images to an identifiable feature, in this case, the sharp edge of the bar.

(a) (b)

Fig. 3. X-ray Fourier transform holograms of the test object recorded at two different angles of incidence: (a) hologram recorded with the object oriented normal to the incident beam, (b) hologram with object oriented at 45° to the beam. The difference in the spatial frequencies of the fringes is visible.

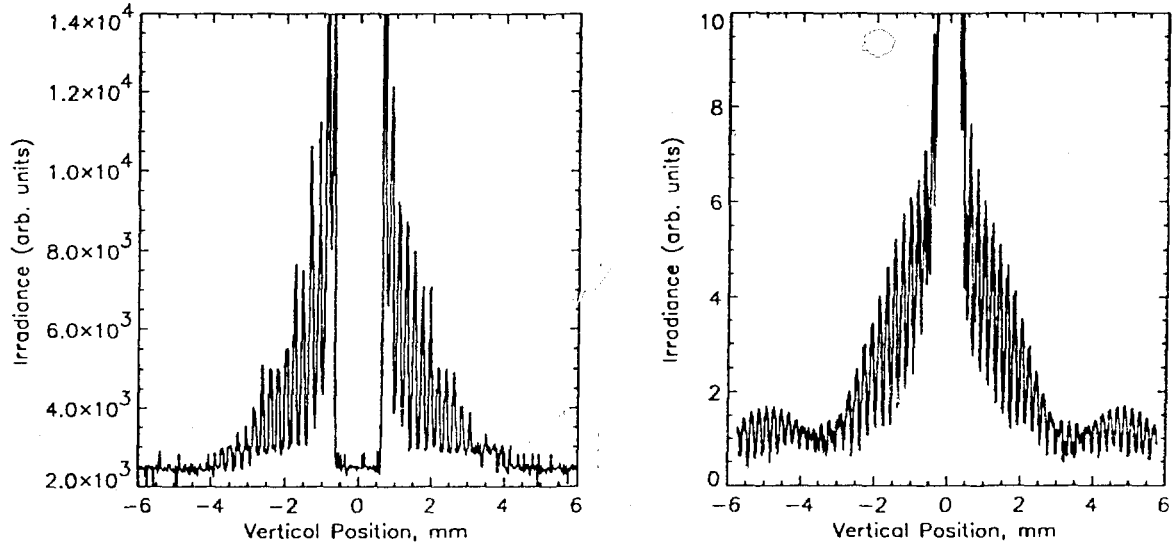

(a) (b)

Fig. 4. Line scans: (a) through x-ray hologram shown in fig. 3(a), and (b) calculated hologram $|a(\xi)|^2$ using Eq. 3. In (a), the beam stop (PCD) blocked the central maximum and the edges of the camera entrance window blocked the second-order peaks.

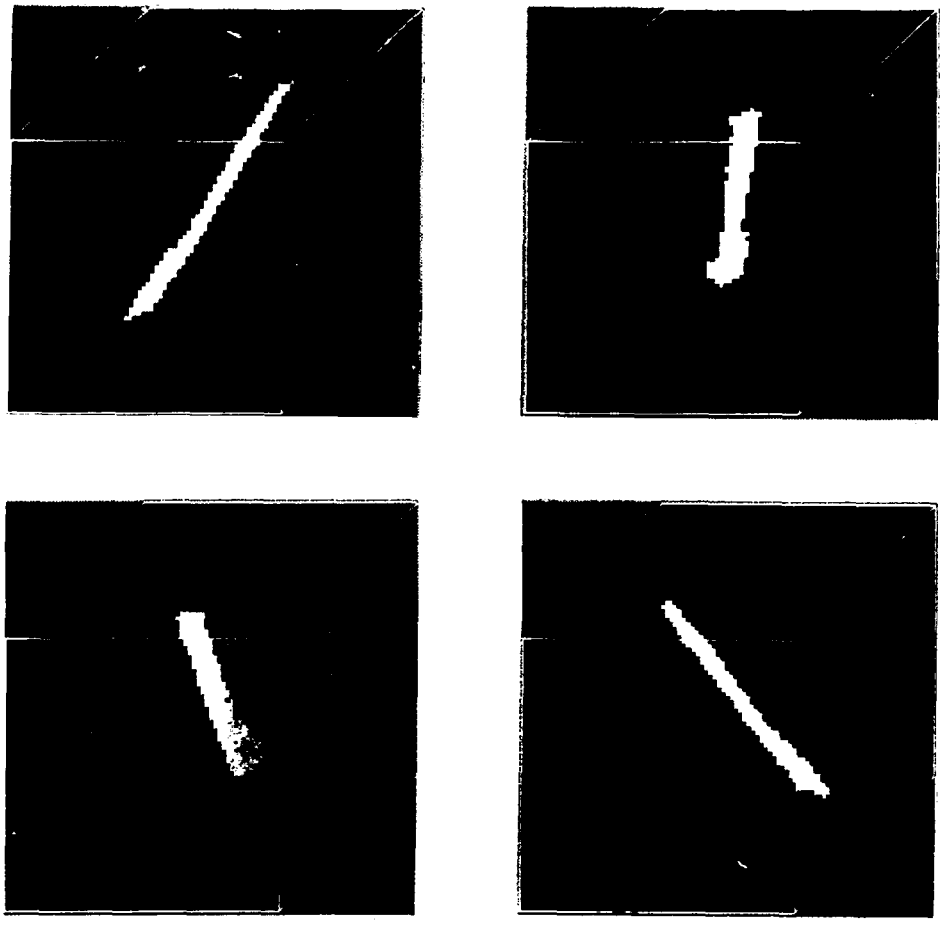

Fig. 5. Numerical reconstructions of a 1-μm segment of the test object, displayed from four arbitrary viewpoints. The bar is well resolved from all sides.

In Fourier transform holography, the precision to which the reference wave is known limits the reconstructible resolution. The curvature of the reference wavefront is related to the numerical aperture, which is given by the wavelength divided by the diameter of the reference source. For the double-bar object,

$$\mathrm{NA} = \frac{\lambda}{2b} \approx 0.025 \tag{4}$$

as the size $D = \lambda z/b$ of the hologram depends on the widths of the bars. This NA gives a depth resolution of $\delta_\ell \sim 5\ \mu\mathrm{m}$ by Eq. 2, which is far greater than the thickness of the object. The 3D reconstructions in Fig. 5 show that the object is significantly better resolved than it would have been had its image been reconstructed from a single hologram. We are currently analyzing the data to quantify the 3D resolution. The preliminary indications are that, for simple objects, the depth resolution approaches the transverse resolution $\delta_t \sim b$ with relatively few views provided that the angular coverage is sufficiently wide.

5. CONCLUSION AND FUTURE DIRECTIONS

There is considerable motivation to develop techniques for three-dimensional x-ray imaging at high spatial resolution. The potential biological and other applications are especially exciting in view of the approaching availability of very high brightness x-ray sources.[20] Diffraction tomography may be a viable avenue toward 3D imaging, provided the number of holographic views required to achieve good depth resolution and the attendent specimen dose can be determined. This work indicates that high resolution 3D x-ray holography is possible with a small number of views, using Fourier transform holography, a high contrast test object and coherent radiation from an undulator source. However, the method has only been tested with one-dimensional objects. Work on 3D x-ray holography of more complex test objects is currently in progress.

7. ACKNOWLEDGEMENTS

We gratefully acknowledge the help of M. Rivers, S. Williams, and S. Wirick, fruitful discussions with J. Kirz and M.R. Howells, and support by D. Attwood. This work was performed under the auspices of the U.S. Department of Energy Advanced Energy Projects Division under contract W-7405-ENG-48, and was carried out at the National Synchrotron Light Source, which is supported by the DOE Office of Basic Energy Sciences. I.M. is additionally supported under contract W-31-109-ENG-38 by the U.S. Department of Energy, BES-Materials Sciences.

8. REFERENCES

1. B.L. Henke, in *Encyclopedia of Microscopy*, G.L. Clark, ed., Reinhold, New York, 1961, p. 675.
2. D. Sayre, J. Kirz, R. Feder, D.M. Kim, and E. Spiller, *Science* **196**, 1339 (1977).
3. M.R. Howells, J. Kirz, and D. Sayre, *Scientific American* **264**, 88 (February 1991).
4. M. Howells, et al., *Science* **238**, 514 (1987).
5. C. Jacobsen, M. Howells, J. Kirz, and S. Rothman, *J. Opt. Soc. Am.* **A7**, 1847 (1990).
6. D. Joyeux and F. Polack, in *OSA Proceedings on Short Wavelength Coherent Radiation: Generation and Applications*, R.W. Falcone and J. Kirz, eds., Opt. Soc. Am., Wash. D.C., 1988, Vol. 2, p. 295.
7. I. McNulty, et al., *Science* **256**, 1009 (1992).
8. J.E. Trebes, et al., *Science* **238**, 517 (1987).
9. D. Gabor, *Proc. Roy. Soc.* **A197**, 454 (1949).
10. G.W. Stroke, *Appl. Phys. Lett.* **6**, 201 (1965).
11. J.T. Winthrop and C.R. Worthington, *Phys. Lett.* **15**, 124 (1965).
12. E. Wolf, *Opt. Commun.* **1**, 153 (1969).
13. A.J. Devaney, in *Inverse Methods in Electromagnetic Imaging, Part 2*, W.-M. Boerner *et al.*, eds., D. Reidel, Dordrecht, 1985, pp. 1107-1135; A.J. Devaney, *Phys. Rev. Lett.* **62**, 2385 (1989).
14. I. McNulty, Ph.D. dissertation, State University of New York, Stony Brook, 1991.
15. H. Rarback, et al., *J. X-Ray Sci. Tech.* **2**, 274 (1990).
16. E.H. Anderson, *SPIE Proc.* **1160**, 2 (1990); E.H. Anderson and D.P. Kern, in *X-Ray Microscopy III*, A.G. Michette, G.R. Morrison, and C.J. Buckley, eds., Springer-Verlag, Berlin, 1992, p. 75.
17. J.W. Goodman, *Introduction to Fourier Optics*, McGraw Hill, San Francisco, 1968, pp. 57-62.
18. J. Brase, T.J. Yorkey, and D.C. Peters, in *X-ray Microimaging for the Life Sciences*, D.T. Attwood and B. Barton, eds., Lawrence Berkeley Laboratory Report **LBL-27660**, 74 (1989).
19. J. Brase, T.J. Yorkey, J.E. Trebes, and I. McNulty, "Image reconstruction for x-ray holographic microscopy," this volume.
20. See for example, *Applications of X-ray Lasers*, R. London, D. Matthews, and S. Suckewer, eds., Lawrence Livermore National Laboratory Report **CONF-9206170** (1992); G.K. Shenoy, P.J. Viccaro, and D.M. Mills, *Characteristics of the 7-GeV Advanced Photon Source: A Guide for Users*, Argonne National Laboratory Report **ANL-88-9**; and *An ALS Handbook*, Lawrence Berkeley Laboratory Report **PUB-643** (1989).

McNulty